IEEE Access
Multidisciplinary ⋮ Rapid Review ⋮ Open Access Journal

Received 15 July 2023, accepted 1 August 2023, date of publication 9 August 2023, date of current version 16 August 2023.

Digital Object Identifier 10.1109/ACCESS.2023.3303842

RESEARCH ARTICLE

A Chemoresistive Gas Sensor Readout Integrated Circuit With Sensor Offset Cancellation Technique

JUN-NYEONG KIM, (Student Member, IEEE), AND HYEON-JUNE KIM, (Life Member, IEEE)
Department of Semiconductor Engineering, Seoul National University of Science and Technology, Seoul 01811, South Korea

Corresponding author: Hyeon-June Kim (hyeonjunekkim@seoultech.ac.kr)

This work was supported in part by the National Research and Development Program through the National Research Foundation of Korea (NRF), Ministry of Science and ICT, under Grant 2022M3H4A1A02076394 and Grant 2022M3I8A2079227; and in part by the IC Design Education Center (IDEC), South Korea, through the EDA Tool.

ABSTRACT This study proposes a chemoresistive gas sensor readout integrated circuit (ROIC) with a simple and effective scheme for tracking and canceling the sensor offset value. Before reading out the gas sensor, the proposed ROIC dynamically updates a of analog-to-digital (A/D) reference range suitable to the gas sensor offset, enabling accurate A/D conversion within the gas sensor's dynamic range (DR). Therefore, this approach eliminates the need for additional complex circuitry or compensation algorithms, allowing the ROIC to extract the desired amount of change effectively. As a result, the overall DR of the gas sensor system is maximized. In addition, the proposed ROIC maintains compatibility with the existing system environment while effectively alleviating the physical limitations of the gas sensor. In terms of commercialization, the effectiveness and feasibility of the proposed ROIC, based on a single-slope A/D converter structure as a readout technique, have been verified. A prototype ROIC was fabricated employing a 180-nm standard CMOS process, exhibiting a total power consumption of 0.5 mW with a conversion rate of 62.5 kSPS. The integrated noise within the range of 1 Hz to 2 kHz was 10.1 μV_{RMS}, corresponding to a DR of 137 dB. Further, the maximum integral non-linearity (INL) was −72.24 dB. The proposed ROIC effectively minimizes sensor offset scattering within 1 LSB of the A/D reference full scale, enhancing performance and feasibility in gas sensor applications.

INDEX TERMS Analog cancellation technique, gas sensor, readout integrated circuit (ROIC), sensor offset tracking, slow response gas sensing system.

I. INTRODUCTION

Gas sensors have found wide application in various Internet of Things (IoT) monitoring systems, such as indoor air quality, water pollution, and exhaled breath monitoring systems [1], [2], [3]. The demand for gas sensors with enhanced performances has been rapidly increasing, leading to the development of different types of gas sensors utilizing various sensing materials, structures, and methods [4], [5], [6]. Among these, metal-oxide-semiconductor (MOS)-based gas sensors have gained attention for IoT applications because of their inherent low cost, compact size, and compatibility with other electronic devices. The chemoresistive characteristics of MOS-based gas sensors simplify the interface circuitry, combining signal conversion and control electronics.

The associate editor coordinating the review of this manuscript and approving it for publication was Wei Wei.

The performance of a gas sensor is evaluated based on many parameters, such as response time, selectivity, recovery time, sensitivity, stability, and fabrication cost [7], [8], [9]. To achieve higher sensing accuracy, extensive research has been conducted to identify optimal materials and physical structures with desired surface and bulk properties. However, improving performance solely through material advancements is challenging due to inherent physical limitations [10], [11]. To overcome the limitations of gas sensors, recent studies have focused on readout integrated circuits (ROICs) employing complex digital signal processing algorithms, leveraging the understanding of gas sensor characteristics [12], [13], [14].

One of the major challenges in extracting output signals from gas sensors using ROICs is the variation in characteristics among different gas sensor samples. Gas sensors also exhibit different chemoresistive characteristics influenced by

environmental factors such as humidity, temperature, and pressure. These factors introduce sensor offset variations, leading to non-uniformity even for the same gas concentration [15]. In most commercial products, this issue is typically addressed through complex digital signal processing and pattern recognition algorithms, which can decrease the price competitiveness. For instance, conventional chemoresistive gas sensors often utilize a Wheatstone bridge sensor circuit with a differential amplifier for resistance-to-voltage conversion [16], [17]. This circuit can only obtain the change amount in the gas sensor compared to a predetermined sensing reference value. However, a critical drawback is that the proper reference value must be manually adjusted upon the change in the gas sensor, which degrades the uniformity and dynamic range (DR) of the entire sensor system. Furthermore, due to the variations in gas sensor offset with environmental changes, designing a cost-efficient circuit is difficult. This restrains its scalability for various applications.

Thus far, based on the analysis of gas sensor properties, various types of sensing methods specialized in ROICs have been reported for effective extraction of the electrical signals in gas sensors [18], [19], [20], [21]. Reference [18] presented a wide dynamic range multi-sensor readout interface, [19] proposed a fast, highly linear, and low-power general-purpose interface circuit, [20] introduced a high-precision, wide dynamic range interface circuit for resistive gas sensor arrays, and [21] presented an analog front-end circuit for interfacing with chemiresistive sensors. Building upon this background, this study proposes a chemoresistive gas sensor ROIC with a simple and effective offset cancellation scheme. The proposed ROIC updates the initial value of an analog-to-digital converter (ADC) before reading out the gas sensor, allowing analog-to-digital (A/D) conversion within the actual DR of the gas sensor. Therefore, this scheme effectively alleviates the sensor offset variation and maximizes the DR of the entire gas-sensor system, eliminating the need for additional complex circuitry or post-signal processing algorithms. In this study, for effectively alleviating the physical limitation of gas sensors, the proposed ROIC based on a single-slope ADC structure [22], [23] was verified for its effectiveness and feasibility.

The remainder of this paper is organized as follows: Section II presents an analysis of the characteristics of the gas sensor offset. Section III describes the proposed ROIC structure and its operation. The measurement results and discussion on the proposed ROIC are presented in Section IV. Finally, the conclusions are presented in Section V.

II. ANALYSIS OF GAS SENSOR OFFSET CHARACTERISTICS

In this section, we focus on the changes in the gas sensor offset characteristics based on the Figaro TGS2600 [15], [16], which is a widely-used commercial MOS-based gas sensor.

Figure 1(a) shows a conventional resistive-divider sensing circuit comprising a gas sensor modeling (R_S) and load resistance (R_L). To reflect the actual resistive characteristics

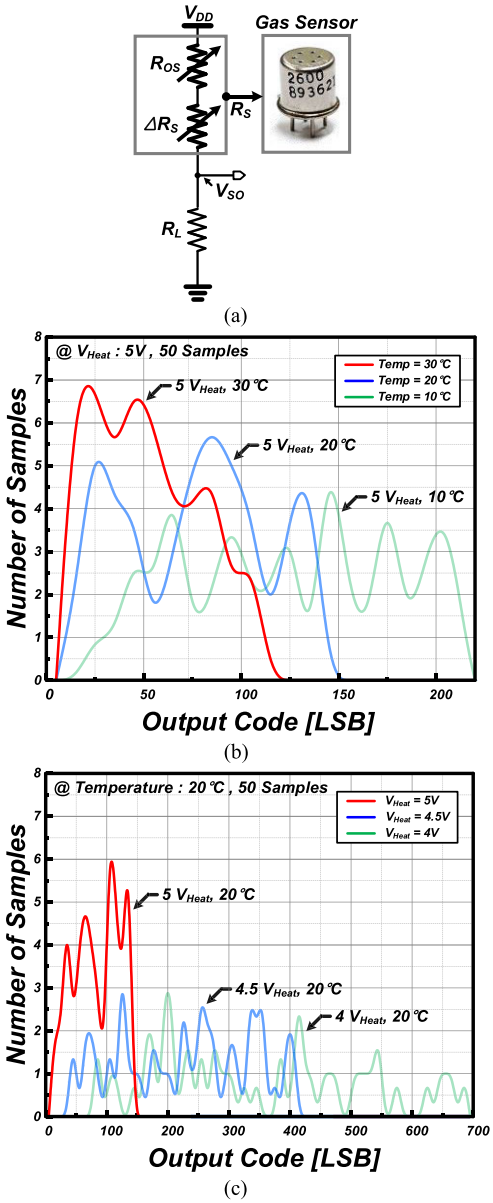

FIGURE 1. (a) Conventional resistive-divider sensing circuit and (b) temperature dependency and (c) Heater voltage dependency of 50 gas sensor samples.

of the gas sensor, the R_S was separated into two parts: the sensor offset (R_{OS}) and the ohmic sensing (R_S) parts. Ideally, it performs resistance-to-voltage conversion, expressed as $V_{SO} = R_L/(\Delta R_S + R_L) \times V_{DD}$, which is established by the relationship among the supply voltage (V_{DD}), ΔR_S, and R_L. The sensor output (V_{SO}) is fed into the ROIC and converted into its corresponding digital code (D_{SO}). In practical scenarios, it is observed that each gas-sensor sample exhibits distinct static characteristics (ΔR_{OS}) that are highly responsive to changes in the surrounding environment. To account for both R_{OS} and ΔR_S, the V_{SO} can be redefined as $R_L / (\Delta R_S + R_{OS} + R_L) \times V_{DD}$. For instance, Figure 1(b) illustrates the dispersion of initial values among 50 gas sensor samples in response to variations in ambient temperature.

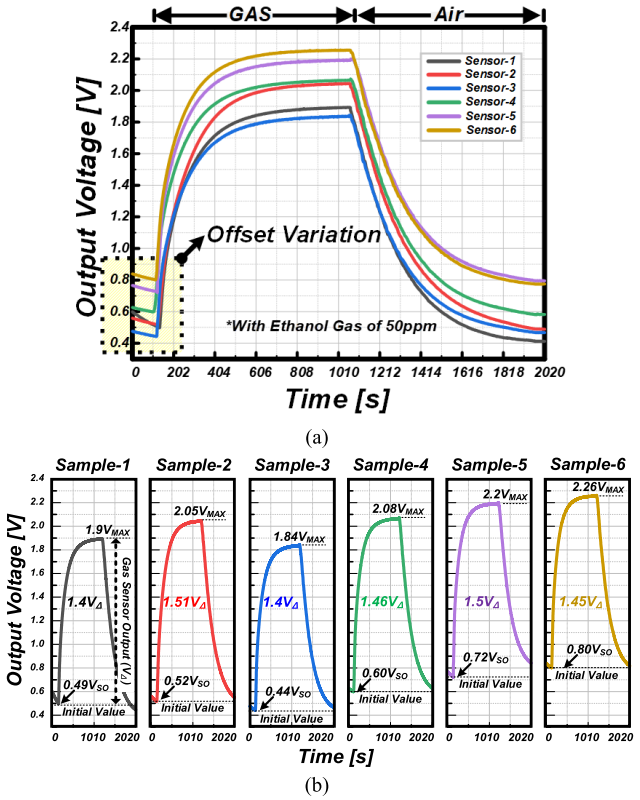

FIGURE 2. (a) Gathered output waveforms from six samples and (b) respective output waveforms.

Here, the X-axis of the plot represents the LSB (Least Significant Bit) values, with a resolution of 11 bits within a 1V full-scale range. It is evident from the figure that the initial value dispersion of the gas sensor significantly changes with temperature fluctuations. Furthermore, even when the gas sensor is subject to heating for activation, there is a notable variation in R_{OS}, leading to the occurrence of ΔR_{OS}, as depicted in Figure 1(c). These observations highlight the influence of temperature and R_{OS} on the gas sensor's initial value dispersion. By considering these factors, we gain a deeper understanding of the behavior and performance characteristics of the gas sensor samples.

To further investigate the effect of ΔR_{OS}, transient output waveforms were gathered from six gas sensor samples, shown in Figure 2. The measurement were conducted by alternately injecting ethanol (50 ppm) and fresh air at a flow rate of 300 sccm. Despite identical measurement conditions, each sensor sample exhibited different results in the range 0.44–0.8 V_{SO} for the initial value ($\Delta V_{SO(Init)}$) and the range 1.84–2.26 V_{MAX} for the maximum value (ΔV_{MAX}), leading to variations in sensing results (V_{Δ}s). These results highlight the importance of minimizing $\Delta V_{SO(Init)}$ caused by ΔR_{OS} to achieve reliable and precise sensing outcomes. In general, post-processing techniques are employed to address this issue; however, they often suffer from complexity and compatibility concerns, negatively impacting price competitiveness. Hence, this study focuses on a method to mitigate the effect of $\Delta V_{SO(Init)}$ to obtain further performance improvements at the system level.

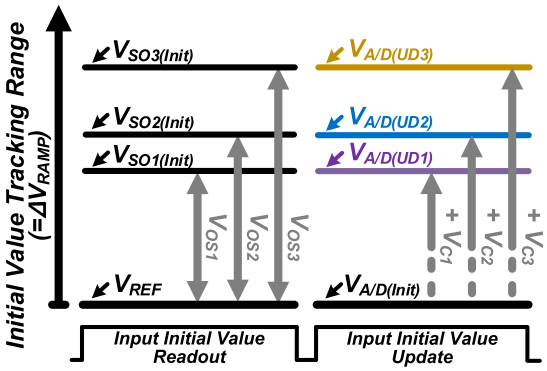

FIGURE 3. Operation principle of proposed gas sensor offset cancellation scheme.

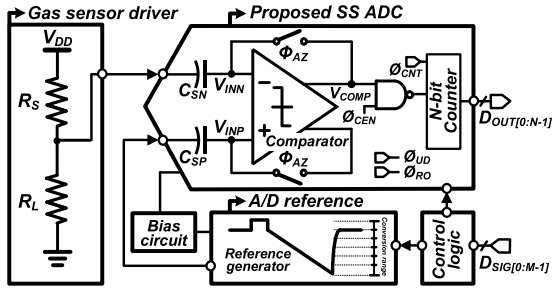

FIGURE 4. Overall circuit block diagram of proposed ROIC.

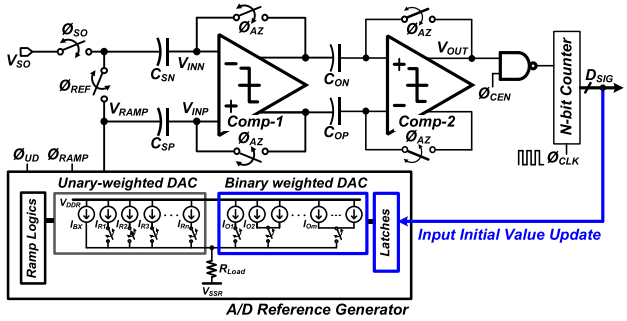

FIGURE 5. Simplified schematic of proposed ROIC with sensor offset cancellation scheme.

III. PROPOSED ROIC DESIGN AND ITS OPERATION

This section introduces a new ROIC design with a sensor offset tracking scheme to address the physical limitations of gas sensors. The design focuses on accurately measuring the change in the gas sensor output within a scaled-down dynamic range (DR), while minimizing the impact of $\Delta V_{SO(Init)}$.

Figure 3 illustrates the operating principle of the proposed sensor offset cancellation scheme, comprising the input initial value readout and updating periods. During the initial value readout period, the ROIC employing the proposed scheme generates V_{OS} by subtracting the reference value (V_{REF}) from the initial sensor output ($V_{SO(Init)}$). This is expressed as $V_{OS} = V_{SO(Init)} - V_{REF}$. Subsequently, the A/D conversion

process begins, resulting in the acquisition of the output digital codes (D_{OS}) that correspond to $V_{SO(Init)}$. Moving on to the initial value update period, D_{OS} is regenerated as the compensation value (V_C) using an additional digital-to-analog converter (DAC) to effectively cancel out V_{OS}. The compensated value, V_C, is then added to the A/D reference value ($V_{A/D(Init)}$), resulting in $V_{A/D(UD)} = V_{A/D(Init)} + V_C$. This can be expressed as $V_{A/D(Init)} = V_{SO(Init)} - V_C$, providing compensation for V_{OS} using V_C. As a result, with the examples of $V_{SO1(Init)}$, $V_{SO2(Init)}$, and $V_{SO3(Init)}$, the proposed scheme enables the effective extraction of the actual changes in the gas sensors within the A/D reference range. In other words, it accurately tracks $V_{SO(Init)}$ to update $V_{A/D(Init)}$ for achieving DR-optimized A/D conversion at a fixed time.

Figure 4 presents the circuit block diagram, encompassing the gas sensor driving circuit, the proposed ROIC with the A/D reference, the biasing circuit, and the control logic. The gas sensor driving circuit produces an output voltage proportional to the resistance variations corresponding to the gas sensor's sensitivity. The proposed ROIC with the A/D reference incorporates a sensor offset removal scheme, where the gas sensor's output voltage is read and processed to eliminate the offset voltage. Consequently, the SS A/D conversion captures only the response variation, converting it into a digital code for precise representation. The control logic ensures synchronized operation of the proposed ROIC, aligning with the timing of ethanol gas injection and fresh air injection. This guarantees proper coordination between gas exposure and refreshment cycles. Finally, the bias circuit generates the requisite currents for circuit functionality.

Figure 5 shows the proposed ROIC, which adopts a sensor offset cancellation scheme. It is based on a typical single-slope (SS) ADC structure [22], [23] that comprises alternating current (AC) coupling capacitors (C_Ss and C_Os), control switches, a comparator, an A/D reference generator, and an N-bit counter. Here, N represents the bit resolution of the ADC. The designed comparator comprises two typical single-ended differential comparators [22]. The gain and 3 dB bandwidth of the comparator were designed to be approximately 98.1 dB and 92 kHz, respectively. The total capacitance of the C_Ss was 1.8 pF, and that of the C_Os was 0.4 pF with a 6.2-fF unit capacitor, wherein a metal–insulator–metal (MiM)-type capacitor was employed. Because the noise performance of the targeted gas sensor (Figaro TGS2600) was not disclosed, in this study, the 12-bit resolution noise requirement was guaranteed. so that the proposed ROIC did not limit the noise performance.

Figure 6 illustrates a simplified operational timing diagram of the proposed ROIC, wherein the sensor offset cancellation period (P_{OC}) and sensor signal readout period (P_{SR}) are depicted. During the P_{OC}, the proposed ROIC functions to read out the $V_{SO(Init)}$ in a manner similar to the existing SS ADC [22]. The conversion result ($D_{SIG(Init)}$) is then updated as the starting point for A/D conversion during P_{SR}, resulting in sensor offset compensation. For a further explanation,

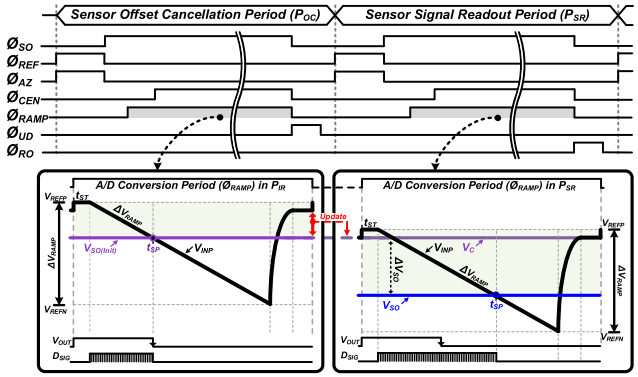

FIGURE 6. Operation principle of proposed sensor offset cancellation scheme.

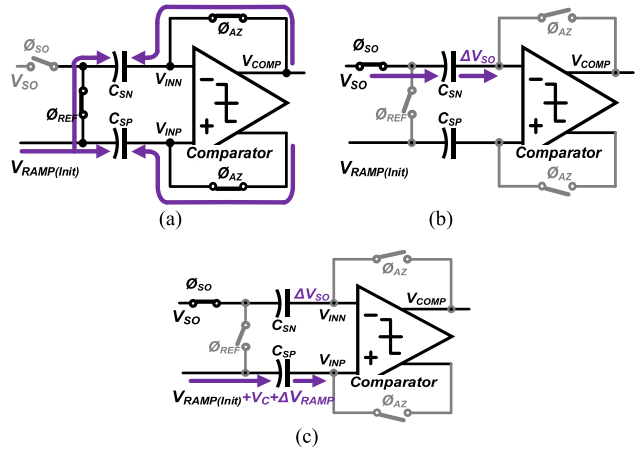

FIGURE 7. Input network of proposed ROIC during the P_{SR}.

Figure 7 shows the input network of the proposed ROIC during the P_{SR}. When the switches $Ø_{AZ}$ and $Ø_{REF}$ are on, as shown in Figure 7(a), the two inputs of V_{INN} and V_{INP} in the comparator reach the same voltage level (V_{COM}). Further, the two sampling capacitors of C_{SN} and C_{SP} sample $V_{COM} - V_{RAMP(Init)}$, respectively. When the switch $Ø_{SO}$ is on, as shown in Figure 7(b), the V_{SO} is coupled through the C_{SN} at node V_{INN}, yielding V_{COM} ($V_{RAMP(Init)} - V_{SO}$); where V_{SO} represents the change in $\Delta V_{SO} + V_{SO(Init)}$. Simultaneously, the V_{INP} node becomes V_{COM} ($V_{RAMP(Init)} - V_C$), where V_C is the value updated in the P_{OC} according to $D_{SIG(Init)}$. When the switch $Ø_{A/D}$ is on, as shown in Figure. 7(c), the A/D reference generator begins to span the full A/D reference scale of V_{REFP}–V_{REFN} (ΔV_{RAMP}), and the counter simultaneously counts the number of ramping steps till the difference between V_{COM} ($V_{RAMP(Init)} - V_{SO}$) and V_{COM} ($V_{RAMP(Init)} + \Delta V_{RAMP} - V_C$). When $\Delta V_{RAMP} \geq \Delta V_{SO}$, the output state of the comparator (V_{OUT}) changes, which then stores the counter status as the conversion result ($D_{SIG(Init)}$). Consequently, as the proposed ROIC performs the A/D conversion based on the $V_{SO(Init)}$, only ΔV_{SO} is effectively extracted without any effects of $\Delta V_{OS(Init)}$. Thus, $\Delta V_{OS(Init)}$ can be minimized via the periodic performing of P_{OC} each time a gas sensor is initialized.

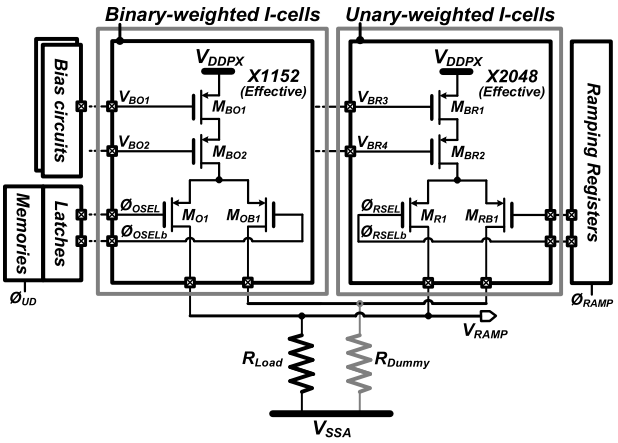

FIGURE 8. Simplified schematic of proposed A/D reference generator.

Figure 8 shows a simplified schematic of the proposed A/D reference generator formed on a typical current-steering DAC structure [24]. It comprises binary-weighted current cells (I-cells), unary-weighted I-cells, load resistors, and peripheral circuits. The unary-weighted I-cells generates ΔV_{RAMP} ($= \sum I_{CELL} \times R_{Load}$) to SS A/D conversion via the sequential application of the I-cells to the R_{Load}. Conversely, the binary-weighted I-cells generates the V_C corresponding to the result of the $D_{SIG(Init)}$ in the P_{OC}. The A/D reference generator requires 3200 I-cells, comprising 128 I-cells for the pre-emphasis period [22], 2048 I-cells to obtain an 11-bit ADC resolution, and 1024 I-cells to cover the $\Delta V_{SO(Init)}$. Consequently, the $D_{SIG(Init)}$ is regenerated as the V_C through the binary-weighted I-cells and added to $V_{RAMP(Init)}$ to update the starting point for the A/D conversion suitable for $V_{SO(Init)}$, resulting in the $V_{SO(Init)}$ compensation effect.

The proposed offset cancellation scheme effectively eliminates the gas sensor offset and accurately measures its changing values. This is achieved by initializing the ADC with the offset value, performing comparisons and adjustments, and compensating the digital output through subtraction of the initial offset value. The proposed scheme utilizes either a SS ADC or a SAR ADC for setting the sensor offset and performing the conversion. When implementing the scheme, the choice between these ADC architectures depends on specific requirements and considerations. The selection of the SS ADC is motivated by the commonly observed low-frequency characteristics in gas sensors, which provide excellent linearity and sensing accuracy. Leveraging these strengths, the proposed scheme with the SS ADC offers a robust solution for effectively mitigating offset effects.

IV. MEASUREMENT RESULTS AND DISCUSSION

Figure 9 depicts the chip microphotograph of this work. A silicon prototype of the proposed ROIC was fabricated using a 180-nm standard CMOS process, which was implemented within an area of 1.81 mm^2. The total power consumption was 0.5 mW, with conversion at 62.5 kSPS. The maximum integral non-linearity (INL) normalized in dB

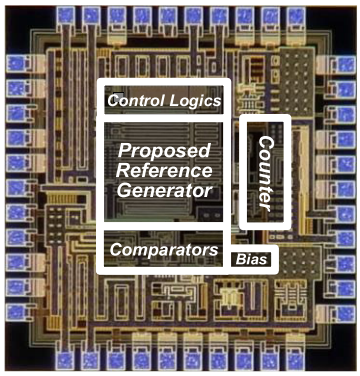

FIGURE 9. Chip microphotograph.

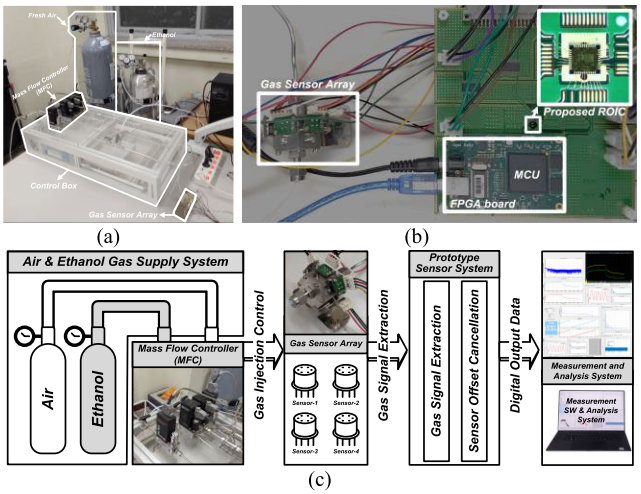

FIGURE 10. (a) Evaluation board with proposed ROIC, (b) test environment setup, and (c) gas measurement flow.

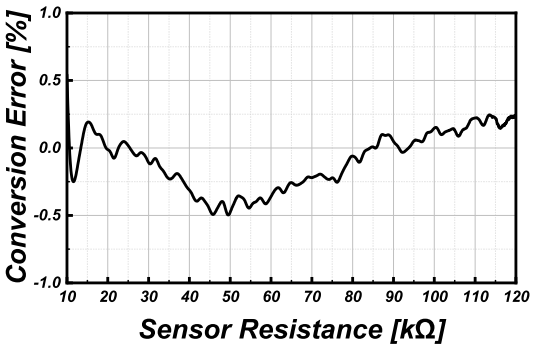

FIGURE 11. Measured conversion error results of proposed ROIC.

with the full-scale value was −72.24 dB, which is effectively 11-bit linearity. Figure 10(a) shows the test environment for ethanol (C_2H_6O) gas sensing at system-level feasibility. It comprises a mass flow controller (MFC) control box with a combination of Line Tech GMC 1000 and M3030V, a Figaro TGS2600 sensor array, fresh air, C_2H_6O gas, and an evaluation board with a customized measurement software program. Figure 10(b) shows a gas sensor array with commercially available Figaro TGS2600 sensors and a customized

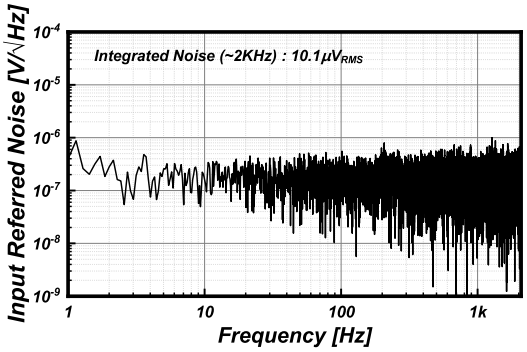

FIGURE 12. Measured input referred noise density of proposed ROIC.

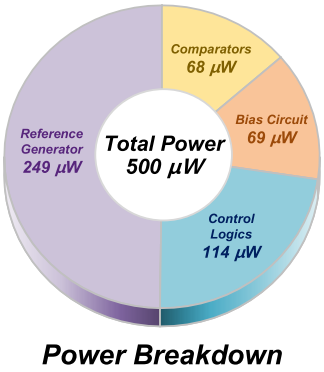

FIGURE 13. Power breakdown of the proposed ROIC.

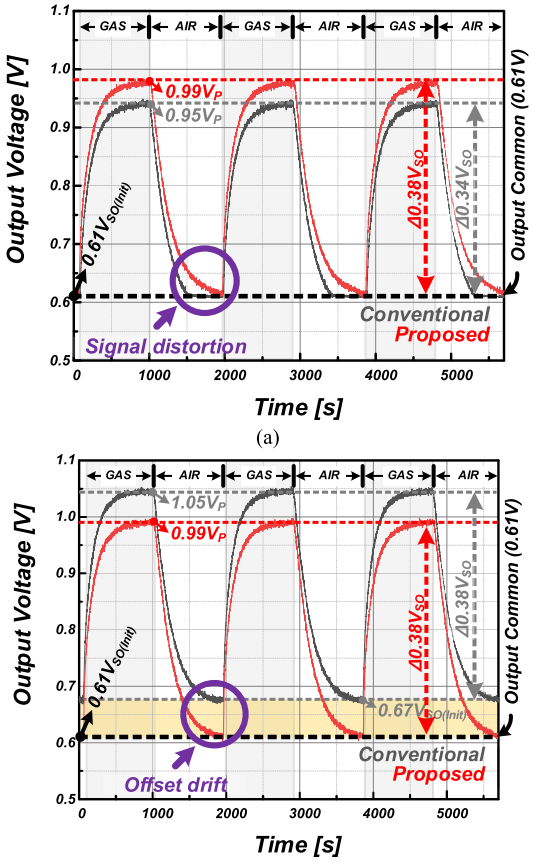

FIGURE 14. Transient waveform results for different two samples of (a) sample-1 and (b) sample-2.

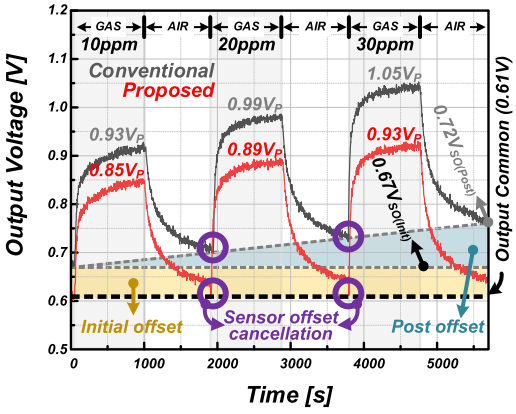

FIGURE 15. Transient waveform results demonstrating effectiveness of the initial offset and post-response offset.

evaluation board assembly with the proposed ROIC and a commercial FPGA (XEM-3050 [25]). Figure 10(c) shows the gas measurement flow. The flow rate was controlled at 150 sccm for C_2H_6O gas at a concentration of 50 ppm and fresh air through the MFC with an injection time of 950 s. The sensor measurements were performed with R_L of approximately 10 kΩ at normal temperature (25 °C ± 2 °C) and relative humidity of R.H. 48 % ± 5 % in fresh air. A test period was performed for 5700 s in three detection cycles. The measured output digital codes of the evaluation board were transmitted to the PC through a USB interface and displayed on the screen in real time. A software program with various verification functions was customized using MATLAB.

Figure 11 shows the measured conversion error plot in the range of the sensor resistance (as specified in Figaro TGS2600 [16]). To generate a test input similar to that of the gas concentrations, the test input with a range of 10–120 kΩ was applied with fixed R_L of 10 kΩ. The proposed ROIC yielded a conversion error of less than 0.5 %, which was maintained even with different sensor samples (i.e., ΔR_{OS}).

The input-referred noise densities were measured and presented in Figure 12, showing an integrated noise of 10.1 μV_{RMS} within the 1 Hz to 2 kHz range at a conversion rate of 4 kSPS. Considering an 11-bit A/D resolution and a 1-V full-scale A/D reference, the LSB value was determined to be 488.3 μV. Importantly, the proposed sensor offset cancellation scheme had no significant effect on the noise figure, thus preserving sensing accuracy. To mitigate 60 Hz power noise, the measurement environment operated on battery power, enabling accurate assessment of ROIC performances. Figure 13 shows the power breakdown of the proposed ROIC.

Figure 14 shows the measured transient waveform results from the conventional (gray) and proposed ROIC (red) for two sensor samples with similar sensitivities but different sensor offsets. Transient waveforms were obtained thrice

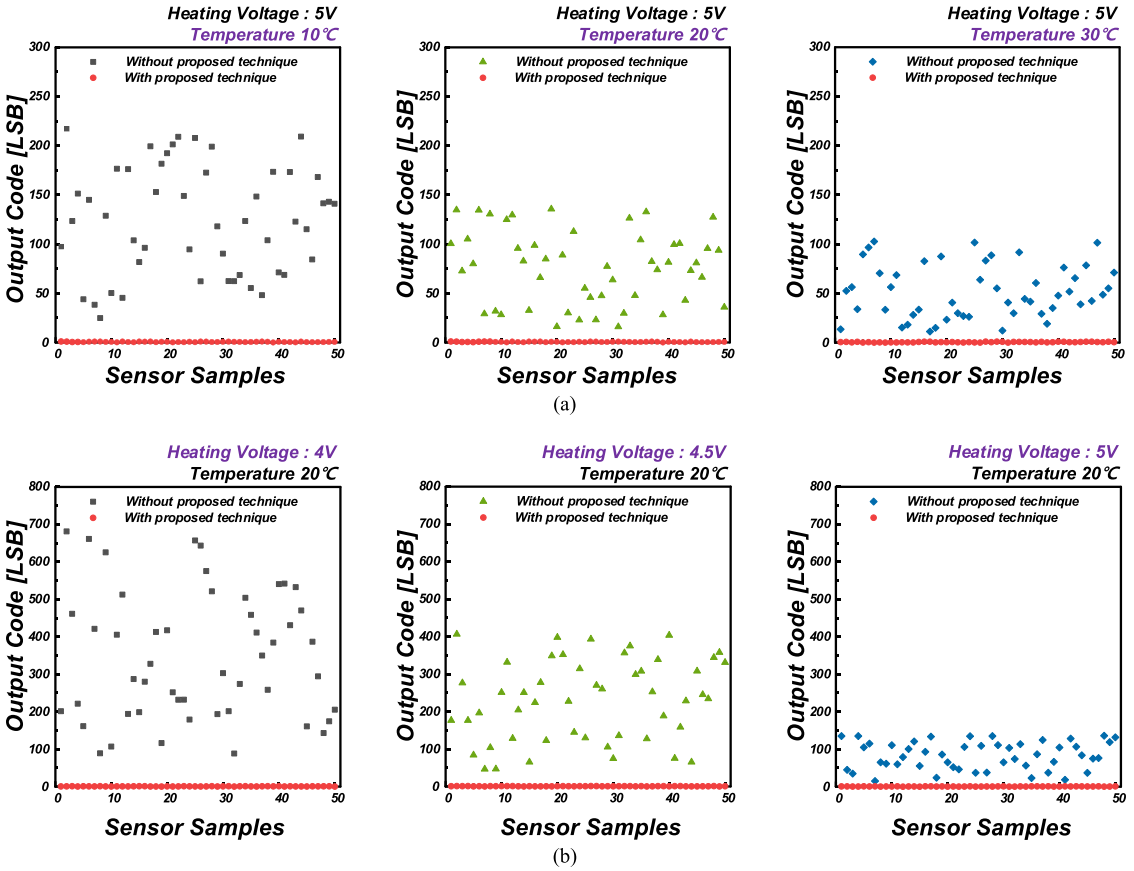

FIGURE 16. Sensor offset scattering plots of fifty TGS2600 samples according to (a) temperature and (b) heating voltage.

through alternately repeated injections of ethanol gas and fresh air. For sample-1 (Figure 14(a)), the conventional ROIC exhibits an output voltage of 0.95 V_P at the initial value of 0.61 $V_{SO(Init)}$. Conversely, for sample-2 (Figure 14(b)), it exhibits an output voltage of 1.05 V_P at the initial value of 0.67 $V_{SO(Init)}$. Because of the different $V_{SO(Init)}$ values of each sample, different outputs were extracted, even at the same gas concentration of 50 ppm. This degraded the discrimination against changes in gas concentration. However, in the case of the proposed ROIC, the initial values of both the samples were maintained at 0.61 V_{Init}. This resulted in sample-1 and sample-2 extracting the same output voltages of 0.99 V_P, which finally yielded the sensing result of Δ0.38 V_{SO}.

Figure 15 presents the results of experiments evaluating the proposed sensor offset calibration scheme. Gas sensor responses were measured using ethanol gas at varying concentrations, with intentional reduction of fresh air to 10 ppm to induce a toxic environment and observe the post-response offset. By increasing the gas concentration from 10 to 30 ppm and repeating the process, we captured the effects of initial offset and post-response offset. A significant difference was observed between the conventional gas sensor and the sensor with the proposed scheme. The conventional sensor exhibited non-linear output due to cumulative offsets caused by initial and post-response factors. In contrast, the proposed scheme effectively mitigated offsets, resulting in a linear output response that accurately reflected gas concentration levels. Figure 15 provide clear evidence of the scheme's effectiveness in extracting sensor response changes and overcoming offset challenges. These findings proves that the proposed ROIC can extract only the amount of change in the V_{SO}, which renders maintaining a high sensing accuracy regardless of any changes in the surrounding environment possible. Moreover, considering that gas sensors have the inherent $\Delta V_{SO(Init)}$ characteristic, it is meaningful that the proposed ROIC minimizes the effect on the difference in $\Delta V_{SO(Init)}$ for each sensor.

To further verify the effectiveness of the proposed ROIC with the sensor offset cancellation scheme, Figure 16 presents the gathered $V_{SO(Init)}$ data of 50 TGS2600 sensor samples plotted against temperature and heating voltage. Without using the proposed scheme, the sensor offset scattering decreased by approximately 56% with an increase in ambient temperature from 10 to 30 °C, and by approximately 74% with an increase in heating voltage from 4 to 5 V. However, with the proposed scheme, the sensor offset scattering was minimized to within 1 LSB of the 11-bit A/D reference full scale, irrespective of changes in the environmental conditions. This result demonstrates that the proposed ROIC significantly alleviates the inherent nonuniformity among the gas sensor samples. Moreover, performing gas sensing at an accurate initial value aids in sensitivity calibration for

TABLE 1. Performance summary and comparison.

PARAMETER	[18]	[19]	[20]	[21]	This work
Technology	0.18 μm CMOS	0.13 μm CMOS	0.35 μm CMOS	0.35 μm CMOS	0.18 μm CMOS
Total area	3.01 mm2	0.125 mm2	3.1 mm2	0.24 mm2	1.81 mm2
Sensing type	Resistance / Current	Resistance	Resistance	Resistance	Resistance
ADC Resolution	12 bits	13 bits	13 bits	11.5 bits (ENOB)	11 bits
Readout speed	100 SPS	4 SPS	100 SPS	1.25 kSPS	62.5 kSPS
Sensing range	7 k ~ 120 kΩ	100 ~ 1 MΩ	100 ~ 20 MΩ	100 ~ 4.7 MΩ	100 ~ 1 MΩ
*Abs. resolution	0.176 Ω	0.4 Ω	0.14 Ω	0.1 Ω	0.5 Ω
Conversion error	-	< 0.4 %	< 0.14 %	< 0.1 %	< 0.5 %
Additional function	Multi-mode sensing	-	Auto-Scaling	Relaxation oscillator-based architecture	Input initial value compensation
**Dynamic range	104 dB	128 dB	160 dB	164 dB	137 dB
Power consumption	0.5 mW	0.68 mW	6 mW	0.37 mW	0.5 mW
***FoM	129 dB	83 dB	93 dB	133 dB	135 dB

*$Abs.\ resolution = R\_min * Converstion\ error$, **$Dynamic\ range = SNDR + 20 * log10\ (Rmax/Rmin)$,
***$FoM = SNDR + 10 * log10(Readout\ speed\ /\ (2 * Power))$, $ENOB = (SNDR - 1.76)\ /\ (6.02)$

each gas sensor. Here, we maintain a controlled environment in a sealed chamber with constant atmospheric pressure and consistent flow rate. Alternating injection of gas and air enables regular measurements, eliminating pressure fluctuation issues.

While the primary focus is on gas sensors, the proposed scheme can also be applied to other types of sensors, such as pressure sensors. By adapting the calibration scheme to pressure characteristics, it becomes possible to mitigate offset variations and improve the accuracy of pressure measurements. The scheme involves extracting the initial offset value of the pressure sensor as a reference point and subtracting it from subsequent measured outputs in real time. This correction ensures more accurate and reliable pressure readings.

The proposed gas sensor offset calibration scheme embedded in the ROIC offers commercial advantages in four key aspects. Firstly, it enables real-time signal calibration, eliminating the need for MCU-based digital post-processing. This enhances processing speed, power efficiency, and system cost-effectiveness. Secondly, the simplicity and versatility of the proposed scheme allow for easy integration with various type of ROIC implementations and potential scalability into other sensor domains. Third, the proposed scheme efficiently removes the gas sensor offset in real-time through the simple circuit technique integrated into the ROIC. This allows for a substantial reduction in DR and, consequently, significant power savings at the system level. Lastly, it significantly benefits gas sensor sensitivity calibration. Calibrating the sensitivity of gas sensors with pre-calibrated initial values can be achieved more easily and with simple digital post-processing using an MCU compared to non-calibrated cases. Based on these reasons, the proposed scheme in this study, with its inherent simplicity and robust advantages, represents a useful and effective method for offset removal in gas sensors within the field.

Table 1 presents the performance of the designed ROIC, including a comparison with previous similar studies [18], [19], [20], [21]. The DR is calculated based on the formulas specified in [19], [26], and [27], resulting in an SNDR of 57 dB and an input impedance range of 100 Ω to 1 MΩ, yielding a DR of approximately 137 dB. The FoM [28], [29] of 135 dB demonstrates a competitive performance compared to other studies. A distinctive feature of the designed ROIC is its built-in function for tracking and calibrating the initial value of the gas sensor. This allows the proposed ROIC to cover the entire output range variation of the gas sensor signal without any loss in DR. By considering the offset dispersion of the gas sensor, the proposed ROIC reduces the unnecessary extension of DR specifications. This is expected to have a significant impact when applied to commercial gas sensors. Additionally, the proposed ROIC maintains compatibility with existing gas-sensing systems while exhibiting competitive performance as a resistive sensor interface. In terms of price competitiveness, the proposed ROIC structure proves to be relatively cost-effective for extracting the amount of change from the gas sensor, as it eliminates the need for additional complex digital circuitry or digital processing implementation.

V. CONCLUSION

This study introduced a new ROIC design with a gas sensor offset cancellation scheme to address the inherent nonuniformity issue among gas sensors. By enabling A/D conversion within the actual DR of gas sensor, the proposed ROIC effectively maximizes the overall DR of the gas sensor system under varying environmental conditions. This enhancement is achieved without the need for additional complex circuitry or post-signal processing algorithms. Further, this study verified the effectiveness and feasibility of the proposed ROIC in overcoming the physical limitations of gas sensors.

REFERENCES

[1] D. Yang, R. A. Gopal, T. Lkhagvaa, and D. Choi, "Metal-oxide gas sensors for exhaled-breath analysis: A review," *Meas. Sci. Technol.*, vol. 32, no. 10, Jul. 2021, Art. no. 102004.

[2] W. Yang, X. Wei, and S. Choi, "A dual-channel, interference-free, bacteria-based biosensor for highly sensitive water quality monitoring," *IEEE Sensors J.*, vol. 16, no. 24, pp. 8672–8677, Dec. 2016.
[3] M. Kampa and E. Castanas, "Human health effects of air pollution," *Environ. Pollut.*, vol. 151, no. 2, pp. 362–367, Jan. 2008.
[4] S. M. Majhi, A. Mirzaei, H. W. Kim, S. S. Kim, and T. W. Kim, "Recent advances in energy-saving chemiresistive gas sensors: A review," *Nano Energy*, vol. 79, Jan. 2021, Art. no. 105369.
[5] P. Srinivasan, M. Ezhilan, A. J. Kulandaisamy, K. J. Babu, and J. B. B. Rayappan, "Room temperature chemiresistive gas sensors: Challenges and strategies—A mini review," *J. Mater. Sci., Mater. Electron.*, vol. 30, no. 17, pp. 15825–15847, Sep. 2019.
[6] A. Dey, "Semiconductor metal oxide gas sensors: A review," *Mater. Sci. Eng., B*, vol. 229, pp. 206–217, Mar. 2018.
[7] N. Barsan, D. Koziej, and U. Weimar, "Metal oxide-based gas sensor research: How to?" *Sens. Actuators B, Chem.*, vol. 121, no. 1, pp. 18–35, Jan. 2007.
[8] T. Zhou and T. Zhang, "Insights into the gas sensor materials: Synthesis, performances and devices," *Sens. Actuators B, Chem.*, vol. 371, Nov. 2022, Art. no. 132565.
[9] H. Ji, W. Zeng, and Y. Li, "Gas sensing mechanisms of metal oxide semiconductors: A focus review," *Nanoscale*, vol. 11, no. 47, pp. 22664–22684, Dec. 2019.
[10] A. Baranov, D. Spirjakin, S. Akbari, and A. Somov, "Optimization of power consumption for gas sensor nodes: A survey," *Sens. Actuators A, Phys.*, vol. 233, pp. 279–289, Sep. 2015.
[11] X. Liu, S. Cheng, H. Liu, S. Hu, D. Zhang, and H. Ning, "A survey on gas sensing technology," *Sensors*, vol. 12, no. 7, pp. 9635–9665, Jul. 2012.
[12] I.-S. Chang, S.-W. Byun, T.-B. Lim, and G.-M. Park, "A study of drift effect in a popular metal oxide sensor and gas recognition using public gas datasets," *IEEE Access*, vol. 11, pp. 26383–26392, 2023, doi: 10.1109/ACCESS.2023.3257414.
[13] D.-Y. Lee, J.-B. Yu, H.-G. Byun, and H.-J. Kim, "Chemoresistive sensor readout circuit design for detecting gases with slow response time characteristics," *Sensors*, vol. 22, no. 3, p. 1102, Jan. 2022.
[14] L. Filipovic and S. Selberherr, "Application of two-dimensional materials towards CMOS-integrated gas sensors," *Nanomaterials*, vol. 12, no. 20, p. 3651, Oct. 2022.
[15] *Figaro Product Information for TGS2600*, Figaro USA Inc, Meadows, IL, USA, Accessed: May 12, 2023. [Online]. Available: https://www.figarosensor.com/product/docs/tgs2600_productinformation%28fusa%29_rev05.pdf
[16] *Figaro Technical Information for TGS2600*, Figaro USA Inc, Meadows, IL, USA,Accessed: May 12, 2023. [Online]. Available: https://www.figarosensor.com/product/data/tgs2600_technical_infomation%28fusa%29_rev03.pdf
[17] A. Somov, E. F. Karpov, E. Karpova, A. Suchkov, S. Mironov, A. Karelin, A. Baranov, and D. Spirjakin, "Compact low power wireless gas sensor node with thermo compensation for ubiquitous deployment," *IEEE Trans. Ind. Informat.*, vol. 11, no. 6, pp. 1660–1670, Dec. 2015.
[18] S. Choi, C. S. Park, H. Y. Chae, B. Oh, J. Lee, Y. M. Kwon, J. M. Baik, H. Shin, and J. J. Kim, "A wide dynamic range multi-sensor ROIC for portable environmental monitoring systems with two-step self-optimization schemes," *IEEE Trans. Circuits Syst. I, Reg. Papers*, vol. 68, no. 6, pp. 2432–2443, Jun. 2021, doi: 10.1109/TCSI.2021.3065503.
[19] F. Ciciotti, C. Buffa, A. V. Radogna, L. Francioso, S. Capone, R. Gaggl, and A. Baschirotto, "A 450-μ a 128-dB dynamic range A/D CMOS interface for MOX gas sensors," *IEEE Sensors J.*, vol. 19, no. 24, pp. 12069–12078, Dec. 2019, doi: 10.1109/JSEN.2019.2939615.
[20] M. Grassi, P. Malcovati, and A. Baschirotto, "A 160 dB equivalent dynamic range auto-scaling interface for resistive gas sensors arrays," *IEEE J. Solid-State Circuits*, vol. 42, no. 3, pp. 518–528, Mar. 2007, doi: 10.1109/JSSC.2006.891724.
[21] A. V. Radogna, S. Capone, L. Francioso, P. A. Siciliano, and S. D'Amico, "A 296 nJ energy-per-measurement relaxation oscillator-based analog front-end for chemiresistive sensors," *IEEE Trans. Circuits Syst. I, Reg. Papers*, vol. 68, no. 3, pp. 1123–1133, Mar. 2021, doi: 10.1109/TCSI.2020.3047508.
[22] H.-J. Kim, "11-bit column-parallel single-slope ADC with first-step half-reference ramping scheme for high-speed CMOS image sensors," *IEEE J. Solid-State Circuits*, vol. 56, no. 7, pp. 2132–2141, Jul. 2021.
[23] M. F. Snoeij, A. J. P. Theuwissen, K. A. A. Makinwa, and J. H. Huijsing, "Multiple-ramp column-parallel ADC architectures for CMOS image sensors," *IEEE J. Solid-State Circuits*, vol. 42, no. 12, pp. 2968–2977, Dec. 2007.
[24] S.-Y. Park and H.-J. Kim, "CMOS image sensor with two-step single-slope ADC using differential ramp generator," *IEEE Trans. Electron Devices*, vol. 68, no. 10, pp. 4966–4971, Oct. 2021.
[25] Opal Kelly Inc. (2014). *PDX. Xem3050 User's Manual*. Accessed: May 12, 2023. [Online]. Available: http://assets00.opalkelly.com/library/XEM3050-UM.pdf
[26] P. Malcovati, M. Grassi, and A. Baschirotto, "Towards high-dynamic range CMOS integrated interface circuits for gas sensors," *Sens. Actuators B, Chem.*, vol. 179, pp. 301–312, Mar. 2013, doi: 10.1016/j.snb.2012.10.019.
[27] M. Grassi, P. Malcovati, and A. Baschirotto, "Fundamental limitations in resistive wide-range gas-sensor interface circuits design," in *Sensors and Microsystems* (Lecture Notes in Electrical Engineering), vol. 54, P. Malcovati, A. Baschirotto, A. d'Amico, and C. Natale, Eds. Dordrecht, The Netherlands: Springer, 2010, pp. 25–40, doi: 10.1007/978-90-481-3606-3_3.
[28] E. Sacco, J. Vergauwen, and G. Gielen, "A 16.1-bit resolution 0.064-mm^2 compact highly digital closed-loop single-VCO-s 1–1 sturdy-MASH resistance-to-digital converter with high robustness in 180-nm CMOS," *IEEE J. Solid-State Circuits*, vol. 55, no. 9, pp. 2456–2467, Sep. 2020, doi: 10.1109/JSSC.2020.2987692.
[29] Y. Lee, B. Cho, C. Lee, J. Kim, and Y. Chae, "A 0.5-ms 47.5-nJ resistor-to-digital converter for resistive BTEX sensor achieving 0.1-to-5 ppb resolution," *IEEE J. Solid-State Circuits*, vol. 58, no. 3, pp. 827–837, Mar. 2023, doi: 10.1109/JSSC.2022.3197549.

JUN-NYEONG KIM (Student Member, IEEE) received the B.S. degree from the Division of Electronics, Information and Communication Engineering, Kangwon National University, Samcheok, South Korea, in 2023. He is currently pursuing the M.S. degree with the Department of Semiconductor Engineering, Seoul National University of Science and Technology, Seoul, South Korea. His current research interests include back-end circuit designs and gas sensor systems.

HYEON-JUNE KIM (Life Member, IEEE) received the B.S. degree from the Kumoh National Institute of Technology, Gumi, South Korea, in 2010, and the M.S. and Ph.D. degrees from the Korea Advanced Institute of Science and Technology, Daejeon, South Korea, in 2012 and 2017, respectively. In 2017, he joined SK Hynix, Icheon, South Korea, where he was worked on the product development of commercial CISs. From 2020 to 2023, he was with the Department of Electronics Engineering, Kangwon National University, Samcheok, South Korea, as an Assistant Professor. He has been with the Department of Semiconductor Engineering, Seoul National University of Science and Technology, Seoul, South Korea, since 2023, where he is currently an Associate Professor. His current research interests include low-power mixed-signal integrated circuits, CMOS image sensors, neuromorphic sensors, and gas sensor systems.